Int J Adv Manuf Technol
DOI 10.1007/s00170-015-7288-7

ORIGINAL ARTICLE

Influence of silver interlayer in dissimilar 6061-T6 aluminum MMC and AISI 304 stainless steel friction welds

P. Kannan[1] · **K. Balamurugan**[2] · **K. Thirunavukkarasu**[3]

Received: 12 June 2012 / Accepted: 7 May 2015
© Springer-Verlag London 2015

Abstract Aluminum MMCs are finding greater utility in automobile and aerospace industries. To boost up the application of aluminum MMCs in real-time applications, it is essential to weld these specimens to other engineering materials. There are several research works reporting the lacuna in arc welding of dissimilar aluminum/steel joints, viz., preferential melting of the aluminum alloy and formation of brittle iron-aluminum intermetallics. However, friction welding process illustrates positive sign for its employment to join dissimilar aluminum/steel. Conversely, intermetallic formation is still of concern. Consequently, to overcome this prevailing problem, interlayers are introduced in this study. At first, dissimilar Aluminum MMCs and AISI 304 stainless steel friction welds are experimented with and without the presence of silver interlayer for conceptual understanding and to clarify and confirm the phenomenal terminologies based on literature. Based on this experience, a few trials of dissimilar Aluminum MMCs and AISI 304 stainless steel friction welds with silver interlayer are experimented on trial and error basis to find optimized friction welding parameter values and these values are used in ANOVA software to plot and analyze the parameters inter dependencies. Then, upper and lower limits of friction welding parameters are fixed to achieve good-quality welds. These limits are fed into ANOVA to obtain full factorial trials based on design of experiment (DoE). The weldments are also evaluated using destructive and non-destructive tests. The metallurgical characterizations of weldments are analyzed. Further, a preliminary attempt is made to develop a finite element model to investigate temperature governing phenomenon such as deformation, stress and strain.

Keywords Friction welding · Aluminum · Stainless steel · Interlayer · ANOVA · Design of experiment · FEM

1 Introduction

Friction welding is defined by the American Welding Society (AWS) as a solid-state joining process in which bonding is produced at temperatures lower than the melting point of the base materials [1]. When two materials, one rotating and another fixed, are pressed against each other at a constant pressure (friction pressure), the temperature of the contacting surface rises due to the heat caused by friction, which forms a high-temperature layer. After the high-temperature layer is formed, the rotation is stopped at once and higher pressure (upset pressure) is applied for a certain period of time. The materials, which are now under high temperature and high pressure, go through a reaction that forms solid-state bonding.

The diffusion bonding and friction welding can be applied directly or with the introduction of an interlayer material at the contact interface [2], and improved weld properties can be achieved by introducing an interlayer between the contacting substrates prior to the friction welding operation. Electron beam welding of aluminum alloy and steel with Ag interlayer was performed [3]. The results revealed that with the rise of the beam offset to the silver side from the interface between silver and steel, the seam morphology was improved, and the porosity in the Ag interlayer perished.

Joints between a 6061-T6 aluminum alloy and a AISI 1018 steel using various parameters were created by inertia friction

✉ P. Kannan
kannan_panneerselvam@yahoo.com

[1] Vivekanandha College of Engineering for Women, Tiruchengode, India

[2] Institute of Road and Transport Technology, Erode, India

[3] TJS College of Engineering, Chennai, India

Published online: 27 May 2015

welding [4], and the joints were evaluated by mechanical testing and metallurgical analysis.

A grain refinement took place in the dynamically recrystallized zone (DXZ) of all the joints. A layered (banded) structure was observed in the DXZs of the joints produced using interlayer, which is formed due to the mixing of two base materials, known as the intercalation of two materials [5]. A hardness reduction usually takes place in the weld region of similar AA6061-T6 and dissimilar AA6061-T6/7075-T6 joints due to solution and/or coarsening of strengthening particles within DXZ and thermomechanically affected zone (TMAZ) and overaging in heat-affected zone (HAZ) region [6]. The loss of strength in the weld region occurs in FSW of aluminum alloys, particularly in age hardened grades, i.e. T6 temper condition, although to an extent it is much lower than those taking place in fusion welds [7–10]. A banded structure consisting of Cr-rich precipitates (σ phase) within the stir zone (SZ) was observed for austenitic steels, i.e. 304 L, which may result in highly degraded corrosion resistance. Type 304 stainless steels often experience similar texture change, i.e. from a copper type rolling texture to a strong cube structure, to Al-alloys during static recrystallization [11, 12].

The grain refinement in the DXZ of O-plates, which is strengthened by solid solution only, results in the increase of strength in that region, whereas the strength undermatching in the weld region of T6 joints occurs due to the dissolution and coarsening of the strengthening particles in these age-hardened plates [13, 14]. Strength overmatching in the weld zone was achieved in O joints contrary to the occurrence of strength undermatching in the weld zone with the joints produced in the aged (i.e. T6-treated) condition [15]. The heat input during welding results in a softening in the HAZ of strain-hardened AA 5754 alloy due to the annealing effect. The softening takes place in the HAZ of AA 2024 alloy, but to a higher degree, due to the reason that the heat input during joining results in overaging in this region [16, 17].

The research work pertaining to interlayers for dissimilar welding is scanty. Added to this, the studies on Al MMCs to stainless steel joining with experimentation, destructive and non-destructive evaluation, analysis on friction welding parameters' interdependencies and finite element modeling and simulation for friction welding process with interlayers have not been reported in detail. Hence, this research study aims at addressing this issue with a systematic approach.

2 Experimental procedure

Experimental trials are conducted for three different cases. Initially, limited experimental trials are carried out based on data available in the literature. This is followed by trials based on trial-and-error method. In the third case, the experimental trials are carried out based on full factorial design obtained using design of experiments (DOE).

Table 1 Parameters and its range for friction welding trials

Trail	Friction pressure (MPa)	Friction time (s)	Forging time (s)	Forging pressure (s)	Rotation speed (RPM)
1	30	4	1	240	1500
2	120	4	1	240	1500
3	240	4	1	240	1500

2.1 Case 1: experiments based on data available in literature

The purpose of this study is to first realize the phenomenon and for conceptual understanding. A limited set of trials are conducted and the corresponding parametric interdependencies observed are reported. Interlayer materials are typically applied during dissimilar friction welding of metal/metal combinations such aluminum and steel base materials [18–21]. The brittle intermetallic layer formation at the bondline is prevented through judicious selection of an interlayer material [2]. The introduction of a 25-μm-thick silver interlayer produced a substantial improvement in tensile strength properties during dissimilar aluminum/stainless steel friction welding [20]. Heat generation during friction welding depends on the applied friction pressure, rotational speed and coefficient of friction [22–24]. Friction time, friction pressure, forging time, forging pressure and rotation speed are the most interesting parameters in friction welding method [25, 26]. All of the process parameters are given in Table 1

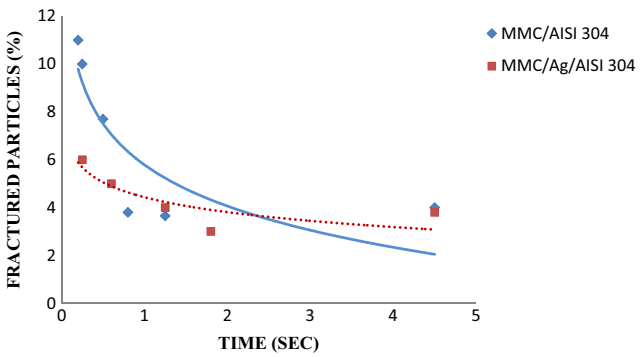


Fig. 1 Percentage of fractured particles in MMC/AISI 304 stainless steel and MMC/Ag/AISI 304 stainless steel friction welds

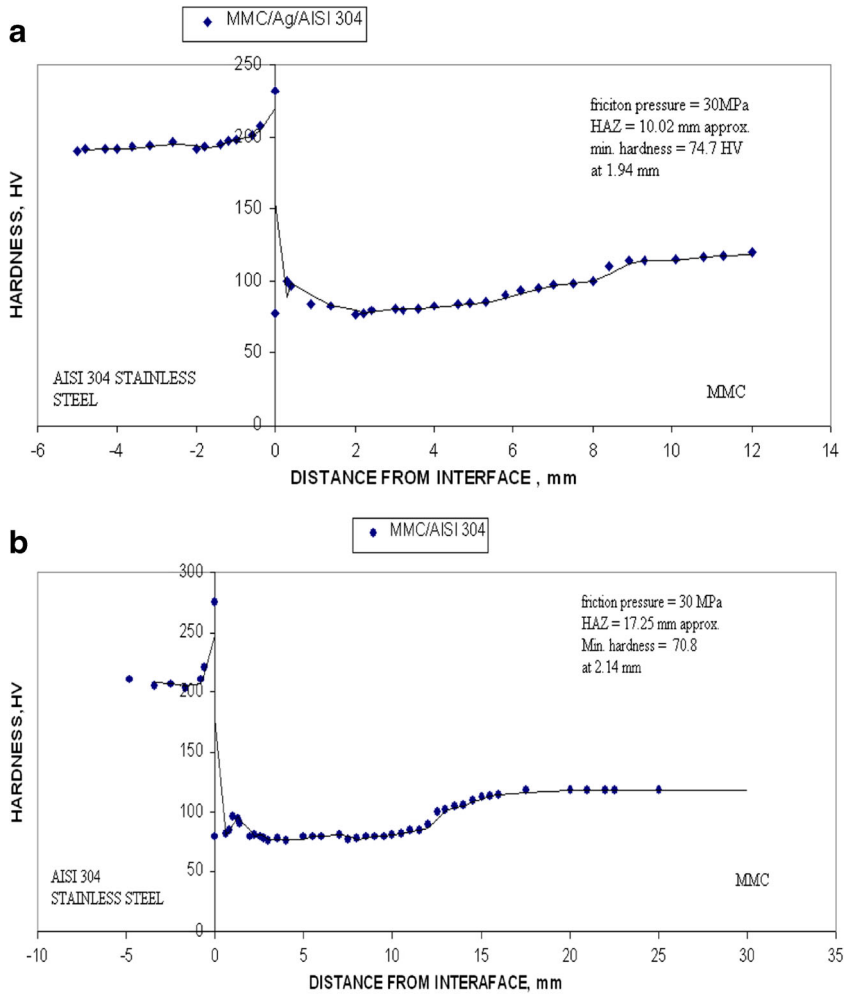


Fig. 2 **a**, **b** Vickers hardness distribution across the joint interface at the friction pressure 30 MPa

2.1.1 Results and discussion

Influence of silver interlayer on particle fracture Introduction of a silver interlayer between the contacting substrates of MMC and AISI 304 stainless steel affected the particle fractures. In MMC/Ag/AISI 304 stainless steel friction joints, the percentage of fractured particles ranged from 6.1 to 2.5 %. But, in MMC/ AISI 304 stainless steel (without silver interlayer) friction welds, particle fracture ranged from 11.1 to 3.8 % (Fig. 1).

Width of the softened zone The dissimilar MMC/Ag/AISI 304 stainless steel friction welds have narrower softened zone than the dissimilar MMC/AISI 304 stainless steel friction joints (Figs. 2, 3 and 4). From Figs. 2, 3 and 4, it is found that the softened zone width ranged from 10.02 mm (welds produced using a friction pressure of 30 MPa) to 3.40 mm (welds produced using a friction pressure of 240 MPa) in dissimilar MMC/Ag/AISI 304 stainless steel welds. But, in dissimilar MMC/AISI 304 stainless steel welds, the width of the softened zone varied from 17.25 to 4.80 mm for the friction pressure ranged from 30 to 240 MPa. So, it is clearly understood that the introduction of silver interlayer reduced the width of the softened zone in the dissimilar MMC/AISI 304 stainless steel friction welds.

2.2 Case 2: experimental trials based on trial and error method

Based on the knowledge obtained from the previous set of experiments, several experimental trials are carried out to create a parameter window and identify the suitable range of parameters which would yield a good-quality weld. Further, levels are fixed for various output phenomenons such as HAZ,

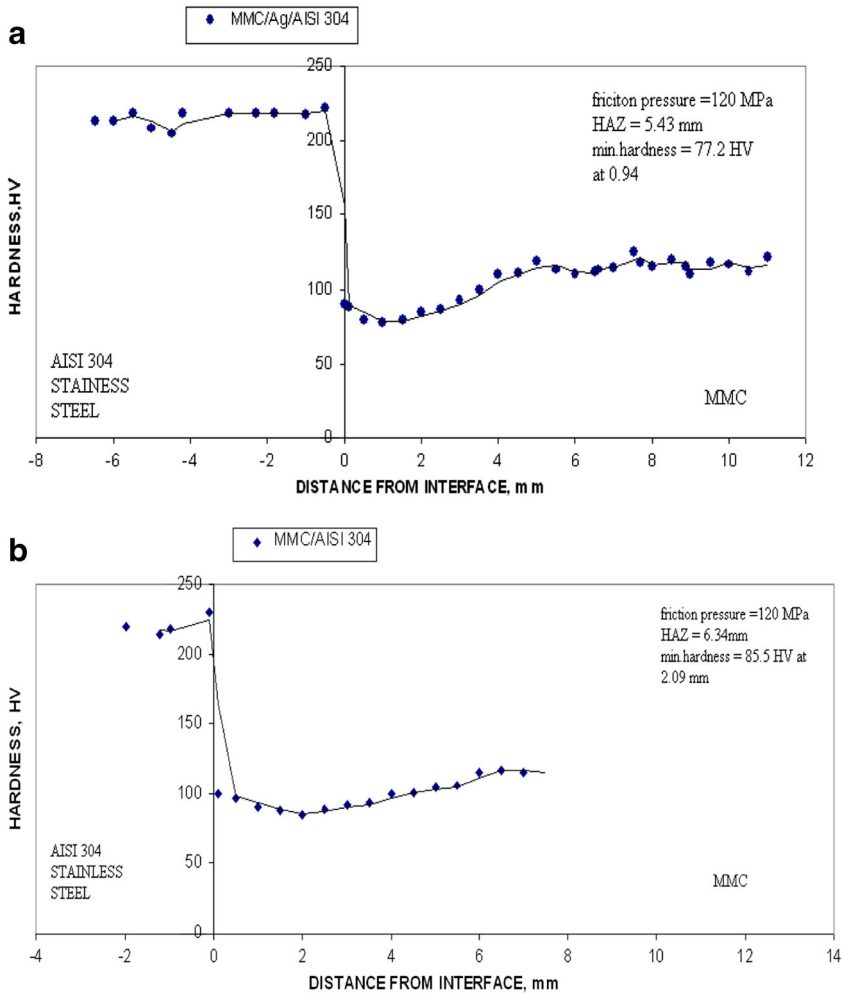


Fig. 3 **a**, **b** Vickers hardness distribution across the joint interface at the friction pressure 120 MPa

stress and weld strength. The objective behind fixing levels is to determine the interdependencies between various governing factors using ANOVA. Table 2 presents the details of the trials carried out.

Three-dimensional plots are obtained by using the data of Table 2 in ANOVA software. These plots provide a clear idea of each parameters influence on the output phenomenons (Fig. 5).

2.3 Case 3: experimental trials based on design of experiments

Table 3 shows the DOE full factorial design based on which the additional experimental trials are carried out. These welded specimens are then evaluated for assessing the strength and quality by subjecting them to destructive, non-destructive testing, respectively. Besides, metallurgical characterization is carried out to understand the weld integrity.

3 Mechanical testing and metallurgical examinations

3.1 Evaluation of mechanical strength through destructive testing

3.1.1 Tensile test

The transverse tensile test is a standard test for procedure qualification and is also used to indicate whether the weld strength equals that of the base metal tensile strength or less [1, 27]. The five weld samples are prepared by using the optimized friction welding parameter values as per Table 3 (trials based on design of

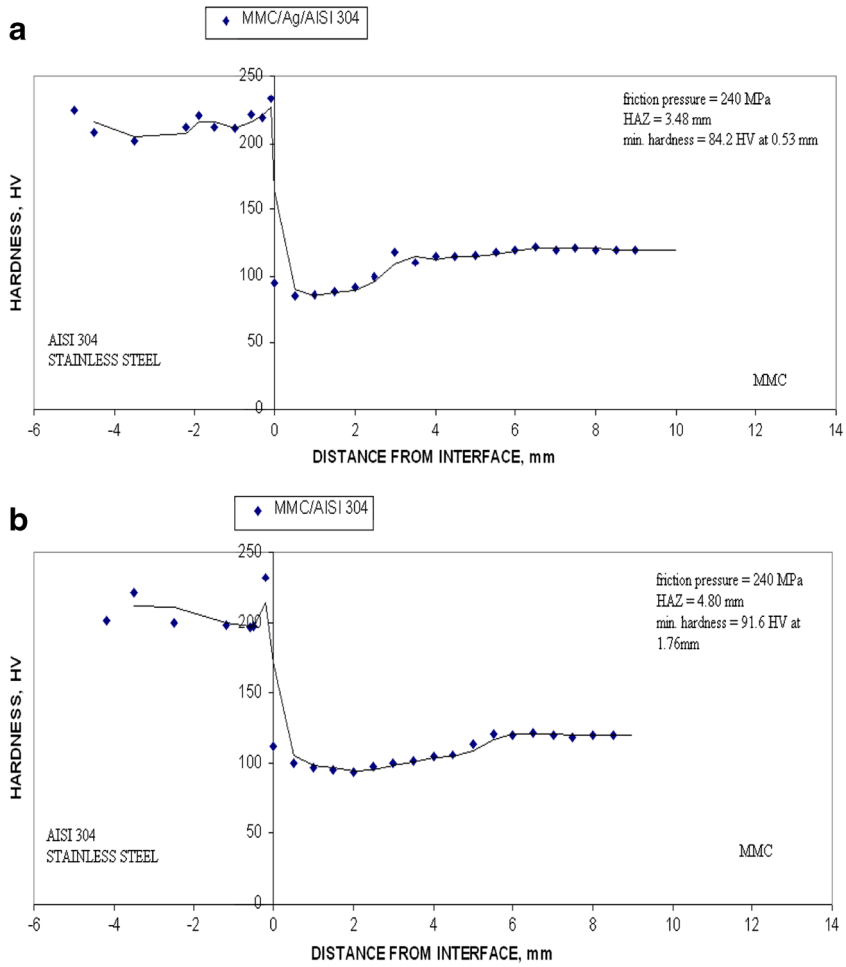


Fig. 4 **a**, **b** Vickers hardness distributions across the joint interface at the friction pressure 240 MPa

experiments). To find the tensile strength of the welded joint, the samples are prepared as per ASTM standards (AWS B4.0). Tensile test is carried out by gripping one end of the specimen in a universal testing machine (UTM) and applying an increasing pull on to the specimen ends till it fractures (Fig. 6).

The tensile test results are given in Table 4 which indicates that the weld strength is slightly above the ultimate tensile strength in the base material of the specimen. Failure in the base material of the specimens in trials indicates that the weld joint is stronger than the base material. The failure of specimen in the weld means that the weld is weaker than the base material. From the tensile tests, we observed that there is no fracture in the weldment, because friction welds were conducted as per the trials based on design of experiments.

3.1.2 Bend test

The quality of the weld, in terms of ductility of the weld metal as well as tests for opening defects particularly lack of side wall fusion, root fusion and penetration of welded joint are most frequently revealed by means of a bend test [27]. For conducting the bend tests, the five weld samples are prepared by using the optimized friction welding parameter values as per Table 3 (trials based on design of experiments). A specimen for bend test prepared as per AWS 4.0 standards shown in Fig. 7. The results of bend test are given in Table 5.

It is observed that all the specimens passed the bend tests and showed no or 1-mm open discontinuity, respectively.

3.2 Non-destructive testing

3.2.1 Radiography test

Radiography is one type of a non-destructive testing technique which may be employed to examine the defects in friction-welded joints [28]. Radiography test of welded specimens does not demand any preparation. The weld region must be cleaned before test is performed.

The quality of the friction welded specimens is assessed using radiography test. Radiography using X-ray is employed to identify and analyze the defects at the friction-welded joint.

Table 2 Trials based on trial and error

Sl. no.	Friction time (s)	Forging time (s)	Forging pressure (Mpa)	Friction pressure (Mpa)	Rotational speed (rpm)	Thickness of inter layer (μm)	Level fixation	HAZ	Level fixation	Weld strength	Level fixation	Stress
1	3	0.8	30	225	1500	2	2	Wider	1	Reasonable	2	High
2	3	0.8	30	225	1500	12	1	Narrow	1	Reasonable	1	Low
3	3	0.8	30	240	1500	2	2	Wider	1	Reasonable	2	High
4	3	0.8	30	240	1500	12	1	Narrow	1	Reasonable	1	Low
5	3	0.8	30	250	1500	2	2	Wider	1	Reasonable	2	High
6	3	0.8	30	250	1500	12	1	Narrow	1	Reasonable	1	Low
7	3	0.8	60	225	1500	2	2	Wider	1	Reasonable	2	High
8	3	0.8	60	225	1500	12	1	Narrow	1	Reasonable	1	Low
9	3	0.8	60	240	1500	2	2	Wider	1	Reasonable	2	High
10	3	0.8	60	240	1500	12	1	Narrow	1	Reasonable	1	Low
11	3	0.8	60	250	1500	2	2	Wider	1	Reasonable	2	High
12	3	0.8	60	250	1500	12	1	Narrow	1	Reasonable	1	Low
13	3	1.5	30	225	1500	2	2	Wider	1	Reasonable	2	High
14	3	1.5	30	225	1500	12	1	Narrow	1	Reasonable	1	Low
15	3	1.5	30	240	1500	2	1	Narrow	1	Reasonable	2	High
16	3	1.5	30	240	1500	12	1	Narrow	1	Reasonable	1	Low
17	3	1.5	30	250	1500	2	1	Narrow	1	Reasonable	2	High
18	3	1.5	30	250	1500	12	1	Narrow	1	Reasonable	1	Low
19	3	1.5	60	225	1500	2	1	Narrow	1	Reasonable	2	High
20	3	1.5	60	225	1500	12	1	Narrow	1	Reasonable	1	Low
21	3	1.5	60	240	1500	2	1	Narrow	1	Reasonable	2	High
22	3	1.5	60	240	1500	12	1	Narrow	2	Good	1	Low
23	3	1.5	60	250	1500	2	1	Narrow	2	Good	2	High
24	3	1.5	60	250	1500	12	1	Narrow	2	Good	1	Low
25	4	0.8	30	225	1500	2	1	Narrow	2	Good	2	High
26	4	0.8	30	225	1500	12	1	Narrow	2	Good	1	Low
27	4	0.8	30	240	1500	2	1	Narrow	2	Good	2	High
28	4	0.8	30	240	1500	12	1	Narrow	2	Good	1	Low
29	4	0.8	30	250	1500	2	1	Narrow	2	Good	2	High
30	4	0.8	30	250	1500	12	1	Narrow	2	Good	1	Low
31	4	0.8	60	225	1500	2	1	Narrow	2	Good	2	High
32	4	0.8	60	225	1500	12	1	Narrow	2	Good	1	Low
33	4	0.8	60	240	1500	2	1	Narrow	2	Good	2	High
34	4	0.8	60	240	1500	12	1	Narrow	2	Good	1	Low
35	4	0.8	60	250	1500	2	1	Narrow	2	Good	2	High
36	4	0.8	60	250	1500	12	1	Narrow	2	Good	1	Low
37	4	1.5	30	225	1500	2	1	Narrow	2	Good	2	High
38	4	1.5	30	225	1500	12	1	Narrow	2	Good	1	Low
39	4	1.5	30	240	1500	2	1	Narrow	2	Good	2	High
40	4	1.5	30	240	1500	12	1	Narrow	2	Good	1	Low
41	4	1.5	30	250	1500	2	1	Narrow	2	Good	2	High
42	4	1.5	30	250	1500	12	1	Narrow	2	Good	1	Low
43	4	1.5	60	225	1500	2	1	Narrow	2	Good	2	High
44	4	1.5	60	225	1500	12	1	Narrow	2	Good	1	Low
45	4	1.5	60	240	1500	2	1	Narrow	2	Good	2	High
46	4	1.5	60	240	1500	12	1	Narrow	2	Good	1	Low
47	4	1.5	60	250	1500	2	1	Narrow	2	Good	2	High
48	4	1.5	60	250	1500	12	1	Narrow	2	Good	1	Low

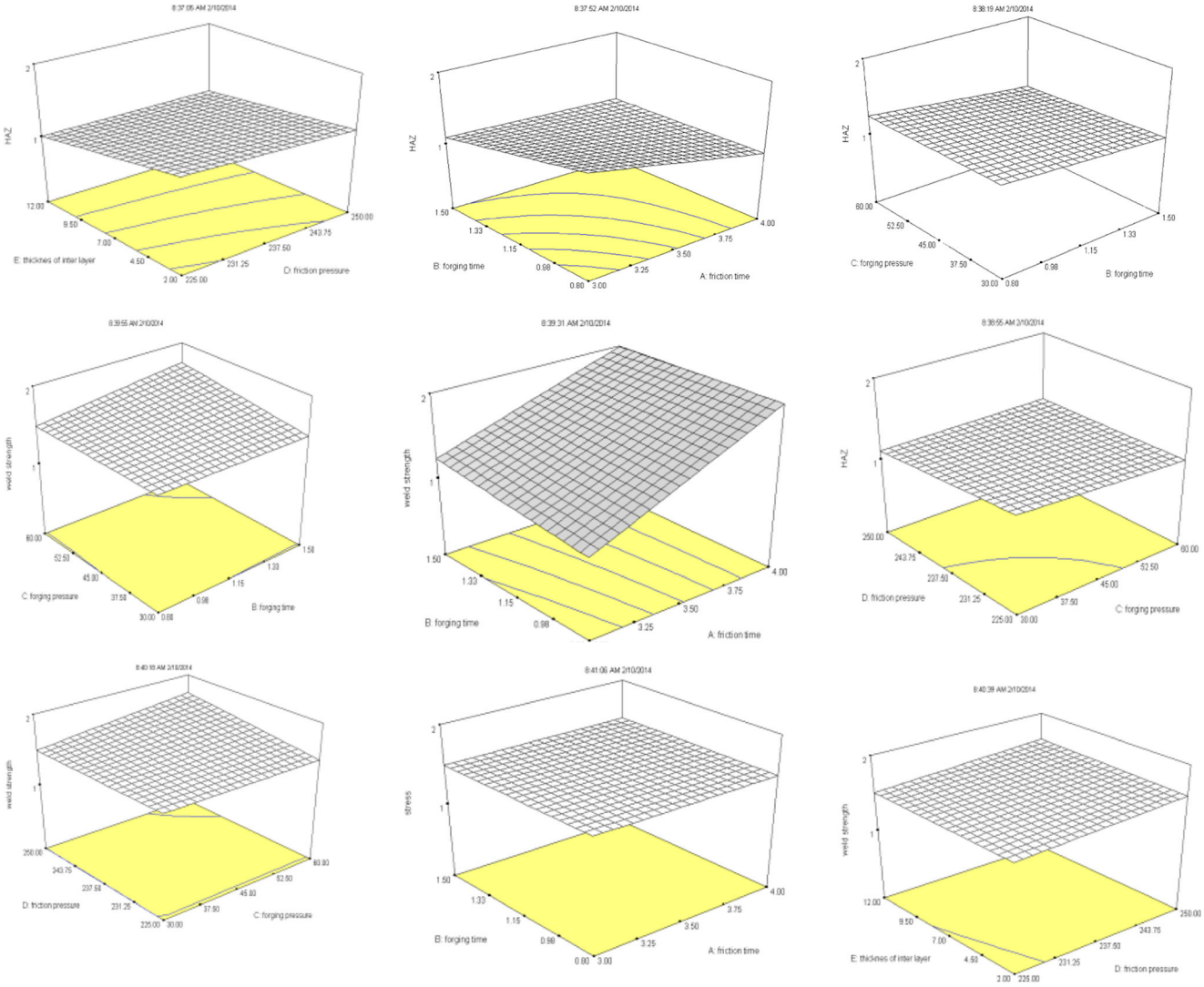


Fig. 5 Three-dimensional parametric plots

From the test results, it is observed that there are only few pores at the weld joint which do not directly affect the quality and is well within the acceptable limits.

3.3 Metallurgical analysis

A few weld samples are completed by using the optimized friction welding parameters as shown in Table 6 according to the trials based on design of experiments for metallurgical examination.

From the extensive metallurgical examinations on the friction-welded specimens, the microstructure of the fusion zone consisting of fine-grained dendritic microstructure precipitates at the grain boundaries is observed. The reason for the formation of this fine grain microstructure in the FZ is the high solidification rates involved which helps retaining the strength of the re-solidified aluminum. No solidification cracking or liquation cracking occurred in the FZ or in the HAZ. A narrow HAZ is formed and the coarsening of the strengthening precipitates in the HAZ is not that pronounced. There was, however, some liquation at the grain boundaries in the FZ and HAZ. Although grain boundary liquation was detected in the FZ and HAZ, no liquation cracking is observed. The joints are stronger than the aluminum parent metal with only a thin diffusion layer at the interface.

Another important observation to note is that the grain boundary liquation becomes more pronounced as the amount of Si along the grain boundaries increases. The overaging in

Table 3 Trials Based on Design of Experiments

Run	Factor 1 A: friction time	Factor 2 B: forging time	Factor 3 C: forging pressure	Factor 4 D: friction pressure	Factor 5 E: thickness	Factor 6 F: rotational speed
1	4	1.2	50	260	12	1500
2	4	1.2	50	260	8	1500
3	4	1.2	50	250	12	1500
4	4	1.5	60	260	8	1500
5	4.25	1	55	255	10	1500
6	4.5	1.5	50	260	8	1500
7	4.25	1.35	66.8	255	10	1500
8	4.25	1.35	55	255	14	1500
9	4	1.5	50	260	12	1500
10	4	1.5	60	250	8	1500
11	4	1.2	50	250	8	1500
12	4.5	1.2	60	260	8	1500
13	4	1.2	60	250	12	1500
14	4.5	1.5	60	260	12	1500
15	4.25	1.35	55	255	10	1500
16	4.25	1.35	55	255	10	1500
17	4	1.5	50	250	12	1500
18	4.25	1.35	55	255	10	1500
19	4.5	1.2	50	250	12	1500
20	4	1.5	50	260	8	1500
21	4.25	1.7	55	255	10	1500
22	4.5	1.5	60	250	8	1500
23	4.5	1.2	50	250	8	1500
24	4	1.2	60	250	8	1500
25	4.25	1.35	55	255	10	1500
26	4.25	1.35	55	255	5	1500
27	4.5	1.2	60	250	8	1500
28	4	1.5	60	250	12	1500
29	4.25	1.35	55	255	10	1500
30	4.8	1.35	55	255	10	1500
31	4.5	1.2	60	260	12	1500
32	4.25	1.35	43	255	10	1500
33	4.5	1.2	60	250	12	1500
34	4	1.5	50	250	8	1500
35	3.6	1.35	55	255	10	1500
36	4.5	1.5	50	250	12	1500
37	4.5	1.5	50	260	12	1500
38	4.5	1.2	50	260	12	1500
39	4.25	1.35	55	255	10	1500
40	4.25	1.35	55	243	10	1500
41	4	1.2	60	260	8	1500
42	4.5	1.2	50	260	8	1500
43	4.5	1.5	60	260	8	1500
44	4	1.2	60	260	12	1500
45	4.25	1.35	55	255	10	1500
46	4.5	1.5	60	250	12	1500
47	4	1.5	60	260	12	1500
48	4.5	1.5	50	250	8	1500
49	4.25	1.35	55	266	10	1500
50	4.25	1.35	55	255	10	1500

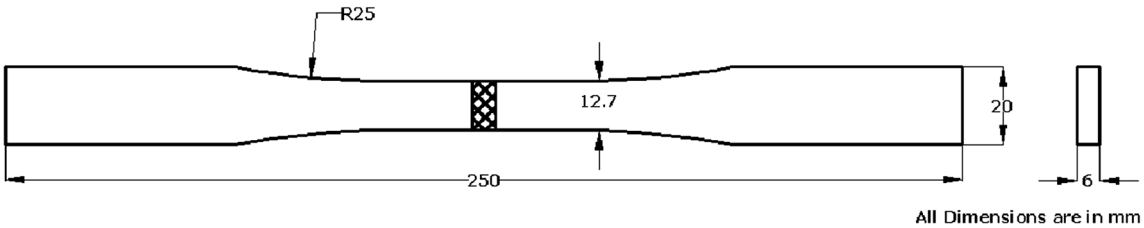


Fig. 6 Friction-welded transverse tensile test specimen

Table 4 Results of tensile test on the friction-welded specimens

Specimen/ material	Specimen size in mm	UTS in MPa	Position of fracture
1	12.7×6.00	456	Base metal
2	12.7×6.00	506	Base metal
3	12.7×6.00	498	Base metal
4	12.7×6.00	493	Base metal
5	12.7×6.00	448	Base metal

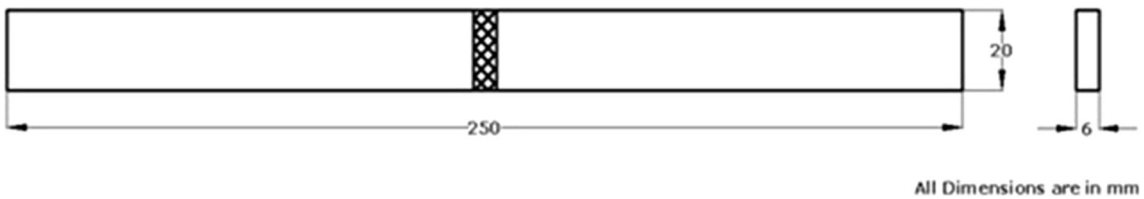


Fig. 7 Friction-welded bend test specimen

Table 5 Bend test results

Specimen	Bend test	Remarks
1	No open discontinuity observed	Passed
2	No open discontinuity observed	Passed
3	1-mm open discontinuity observed	Passed
4	No open discontinuity observed	Passed
5	1-mm open discontinuity observed	Passed

Table 6 Friction-welded specimens with friction welding parameters for metallurgical examination

Specimen	Factor 1 A: friction time	Factor 2 B: forging time	Factor 3 C: forging pressure	Factor 4 D: friction pressure	Factor 5 E: thickness	Factor 6 F: rotational speed
1	4	1.2	50	260	12	1500
2	4	1.2	50	260	8	1500
3	4.25	1	55	255	10	1500

the HAZ region of the welding leads to a decrease in the strength of HAZ while the strength of the fusion zone is restored to the level of the heat-affected zone. The acceptable level of cracking, debonding and porosity were determined in the joints produced. However, no weld-defect formation took place in the weld regions of all the joints produced (Figs. 8, 9, 10, 11, 12, 13, 14, 15 and 16).

3.3.1 Metallurgical examination on specimen 1

A: friction time (s)	B: forging time (s)	C: forging pressure (Mpa)	D: friction pressure (Mpa)	E: thickness (μm)	F: rotational speed (rpm)
4	1.2	50	260	12	1500

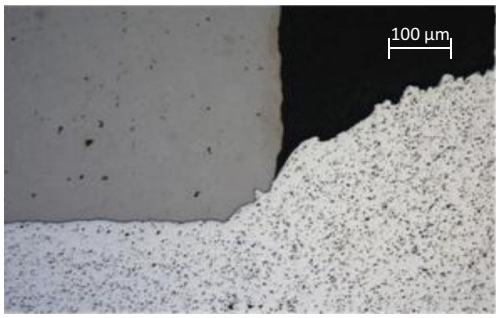


Fig. 8 Fusion line of the friction welded specimen 1

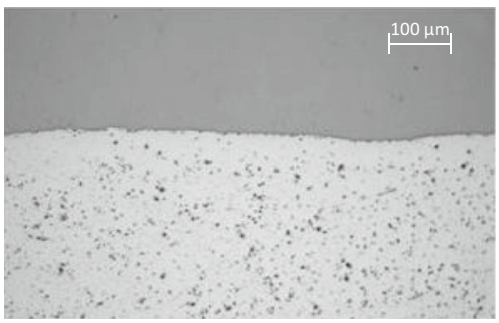


Fig. 9 Weld interface of the friction-welded specimen 1

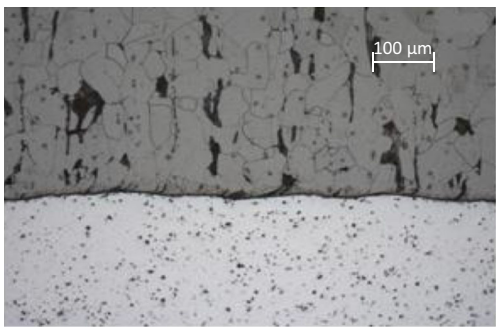


Fig. 10 SEM micrograph of the friction-welded specimen 1

3.3.2 Metallurgical examination on specimen 2

A: friction time (s)	B: forging time (sec)	C: forging pressure (Mpa)	D: friction pressure (Mpa)	E: thickness (μm)	F: rotational speed (rpm)
4	1.2	50	260	8	1500

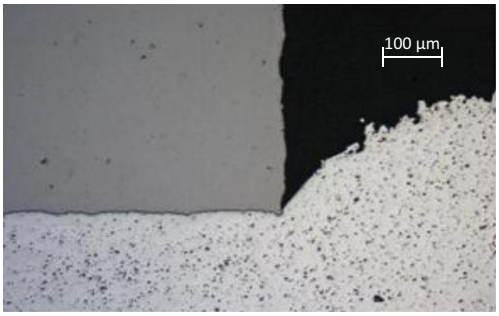


Fig. 11 Fusion line of the friction-welded specimen 2

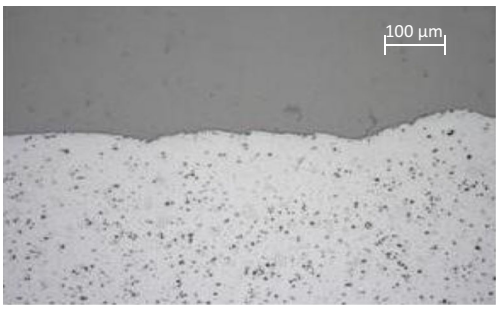


Fig. 12 Weld interface of the friction-welded specimen 2

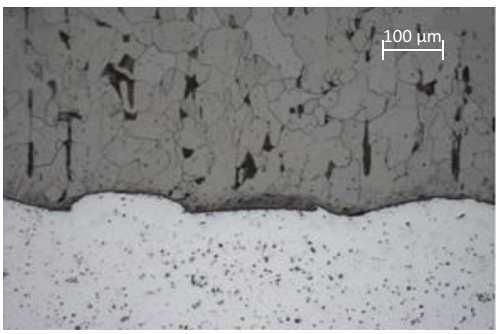


Fig. 13 SEM micrograph of the friction-welded specimen 2

3.3.3 Metallurgical examination on specimen 3

A: friction time (s)	B: forging time (s)	C: forging pressure (Mpa)	D: friction pressure (Mpa)	E: thickness (μm)	F: rotational speed (rpm)
4.25	1	55	255	10	1500

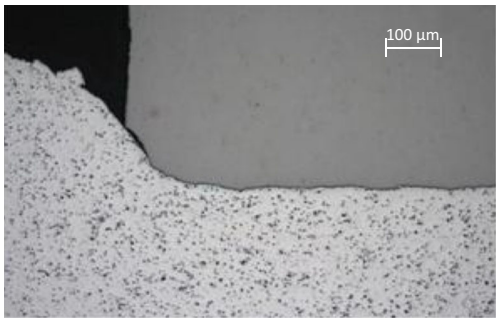


Fig. 14 Fusion line of the friction-welded specimen 3

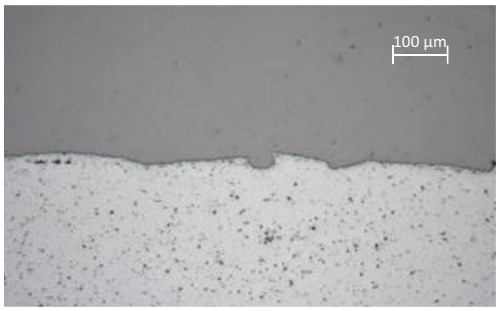


Fig. 15 Weld interface of the friction-welded specimen 3

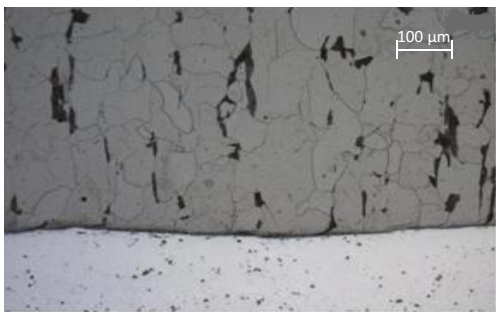


Fig. 16 SEM micrograph of the friction-welded specimen 3

4 FEM for friction welding of rods with silver interlayer

The material properties of the aluminum alloy, stainless steel and silver are used for the FEM analysis.

4.1 Boundary condition and heat input

For this study, an assumption is made that the friction welding process is carried out at room temperature with air as the medium in the setup. The necessary mathematical equations for the FEA are adopted here.

4.2 Results and discussion

4.2.1 Deformation analysis

A unique pattern and characteristic is prevalent as shown in Fig. 17 and is described as follows: At a very far distance from the weld centerline, the von Mises stress is found to be similar to the von Mises stress of material at room temperature, since the effects of temperature and deformation on the material are negligible. At a closer distance to the weld centerline, in the heat-affected zone, the temperature increases and the yield stress at temperature decreases which, in turn, reduces the von Mises stress. At a closer distance to the weld centerline, the increase of temperature produces more plasticity while the rest of the material resists against the deformation which, in turn, increases the von Mises stress. At the weld centerline, where the two surfaces are in contact with each other, the von Mises stress reduces and the peak plastic strain increases due to temperature softening produced at the weld centerline. At distances away from the weld zones due to resistance of the material against the deformation, the von Mises stress increases.

The von Mises stress obtained for the friction welding of aluminum alloy and stainless steel is found to be higher than that of the individual materials. This matter is attributed to friction welding of two dissimilar materials, which in turn produces more resistance to deformation due to the materials' yield stress variations at temperatures. The deformation is observed to be prominent along x-axis and z-axis with its value ranging between 3.67 and 3.73 units at the weld line possessing silver interlayer. The deformation increase while moving towards aluminum alloy and contrarily decreases towards the stainless steel rod.

4.2.2 Stress analysis

In the friction welding process, continuous rubbing of contact surfaces generates the heat at the weld interface. The temperature of the material increases with heat and therefore subsequent softening of the material occurs. The material at the interface starts to flow plastically and forms an upset collar (Fig. 18).

Simulation results show that the final pressure does not significantly affect the stress obtained at the fusion zone and on the fixed bar. However, the stress increases slightly in the rotating bar with the final pressure. In other words, the HAZ stress increases in the rotating bar with the final pressure. Figures reveal that initial pressure is a more important parameter than final pressure in affecting the stress. The stress induced is observed to be 280 units in the weld line in the presence of silver interlayer. While on other portions, the stress appears to decrease. However, in the aluminum alloy rod the stress is reasonably higher than in the steel rod.

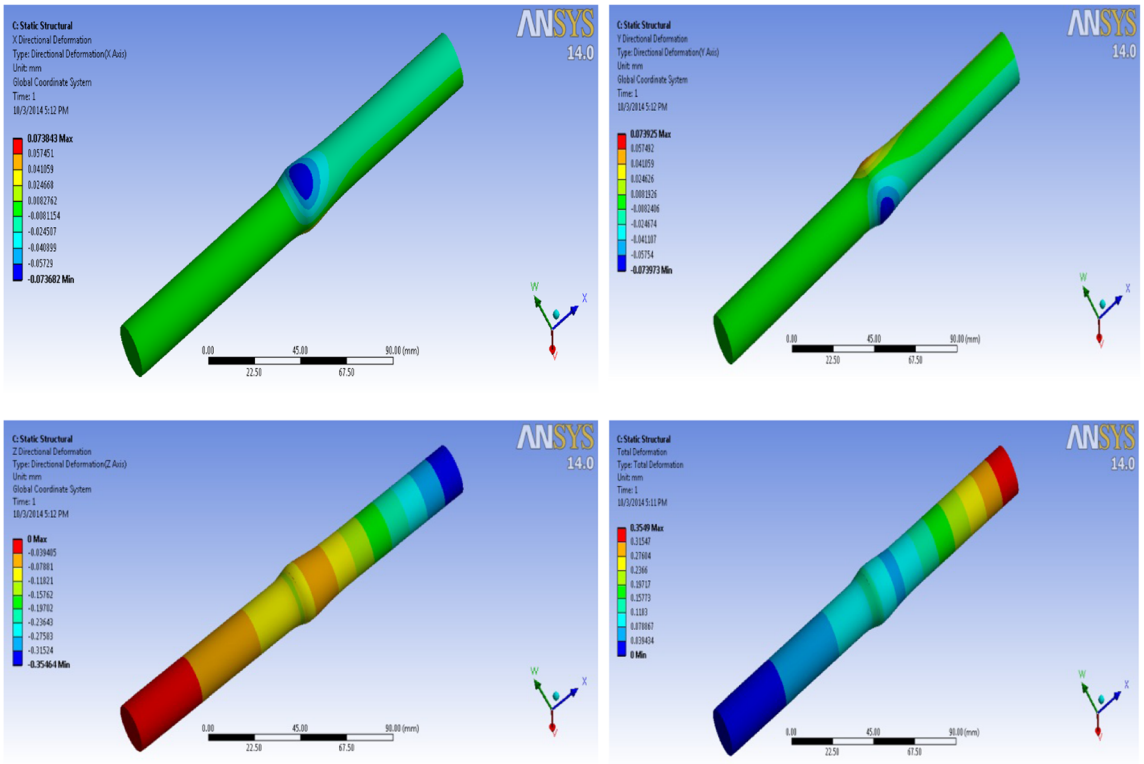


Fig. 17 Deformation along different axes and total deformation

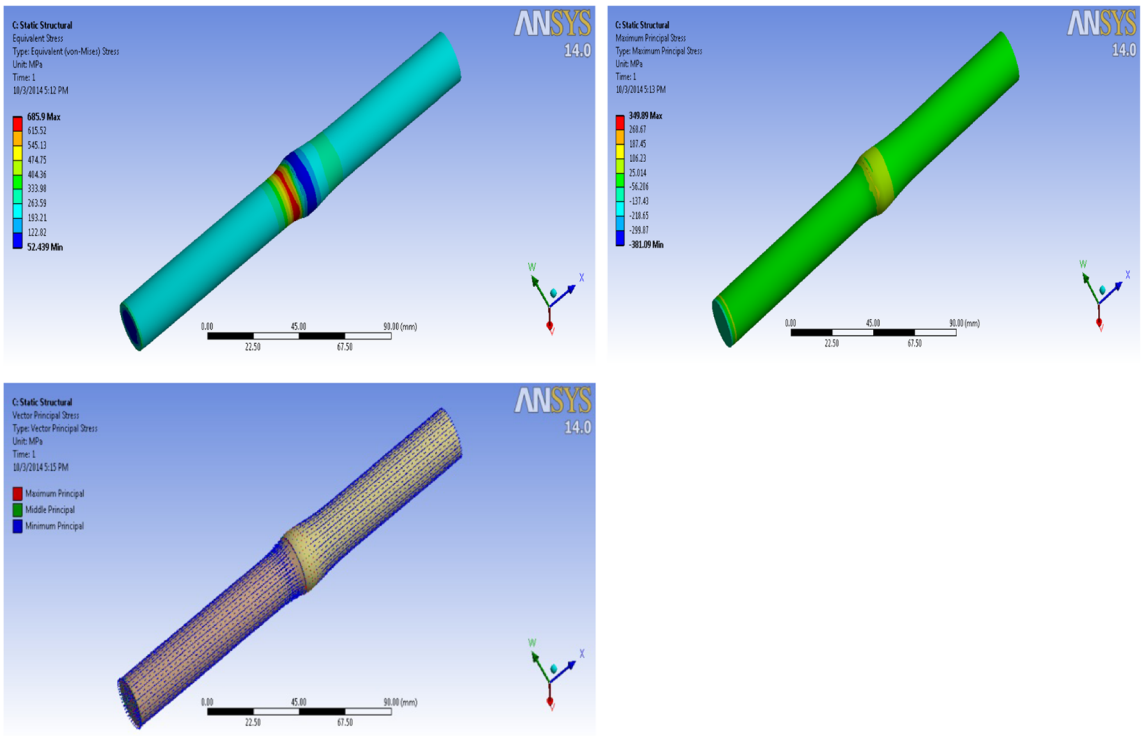


Fig. 18 Induced stresses in the welded rods

4.2.3 Strain analysis

Figure 19 shows the strain rate distributions for friction welding of aluminum alloys and stainless steel materials. Strain rate variations are wider than those for similar materials friction weld.

However, Fig. 19 shows that the strain rate is zero at the weld interface due to temperature softening and might be positive and negative in the heat-affected zone, decreasing from zero to a minimum value and reaching again at $x=0$, to rise to a maximum positive at the heat-affected zone. This variation of the strain rate is seen in modeling of all samples. The strain rate approaches zero at a far distance since no deformation occurred at distances away from the weld and HAZ regions. More fluctuation of the strain rate was observed in the material's left-hand side than in the right-hand side. The reason is attributed to fixing of the right-hand-side bar and rotation of the left-hand-side bar. The strain rate fluctuations are increased with the bar rotation velocity. The simulation results show that the effective strain distributions are not affected by the final pressure. Figure 19 reveals that initial pressure is more effective than final pressure on changing the effective strain profiles. The strain is higher in the steel rod and decreases while moving towards aluminum alloy rod with 1.002 units induced at the weld line with silver interlayer.

5 Conclusions

On the basis of this study, the following conclusions can be drawn.

- The introduction of silver interlayer reduced the percentage of fractured particles and also the width of softened zone at the bondline.
- The percentage of reinforcing particles in the MMC/AISI 304 stainless steel joints ranges from 11.1 to 3.8 % particle fracture. After the introduction of silver interlayer, the percentage of reinforced particles ranges from 6.1 to 2.5 % particle fracture. Therefore, the introduction of silver interlayer shows 3.15 % decrease in particle fracture when compared to normal friction welding process.
- The experimental trials based on trial-and-error method find the optimized friction welding parameters. Friction welding parameters' interdependencies are also plotted and analyzed using ANOVA. Further, the range of parameters are fixed and fed into ANOVA to get full factorial trials based on the design of experiment.
- The mechanical testing and metallurgical characterizations of the friction welded joints with interlayers reveal higher strength, hardness, better micro structural integrity and good quality.
- Simulation results predict a high value of plastic strain produced at the weld centerline due to increasing the

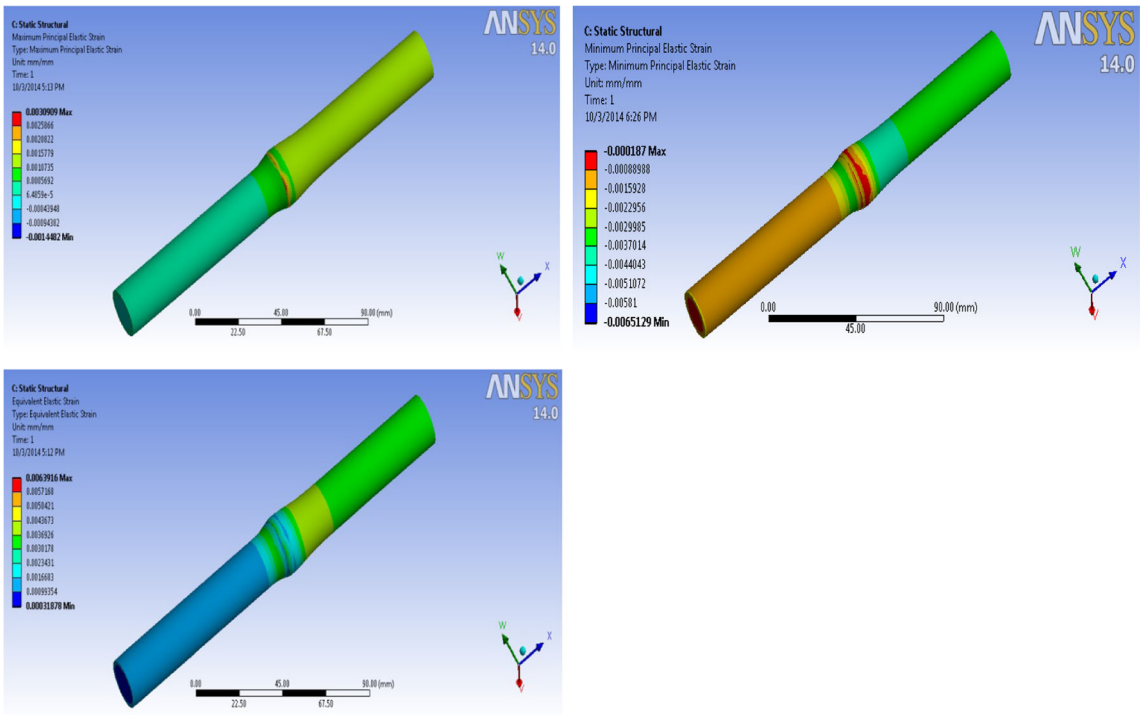


Fig. 19 Induced strains in welded rods

temperature. The peak von Mises stress is produced at distances away from the weld centerlines. The von Mises stress reduces in the fusion zone due to temperature softening. The von Mises stress obtained for friction welding of steel to aluminum alloys is found to be high. This is attributed to friction welding of two dissimilar materials, which in turn, produces more resistance to deformation, and is also due to the materials yield stress variations at temperatures.

References

1. Maldonado C, North TH (2001) Softened zone formation and joint strength properties in dissimilar friction welds. J Mater Sci 37(10): 2087–2095
2. Elliot S, Wallach ER (1981) Metal Constr 13(3):167–171
3. Zhang B-G, Shi M-X, Chen G-Q, Feng J-C (2012) Microstructure and defect of titanium alloy electron beam deep penetration welded joint. Elsevier, Science Press, Science Direct, Trans. Nonferrous Met. Soc China 22(11):2633–2637
4. Taban E, Gould JE, Lippold JC (2010) Dissimilar friction welding of 6061-T6 aluminum and AISI 1018 steel: properties and microstructural characterization. Mater Des 31(5):2305–2311
5. Çam G, İpekoğlu G, Serindağ HT (2014) Effects of use of higher strength interlayer and external cooling on properties of friction stir welded AA6061-T6 joints. Sci Technol Weld Join 19(8):715–720
6. İpekoğlu G, Erim S, Gören Kıral B, Çam G (2013) Investigation into the effect of temper condition on friction stir weldability of AA6061 Al-alloy plates. Kovove Mater 51(3):155–163
7. Cam G, Kocak M (2007) Microstructural and mechanical characterization of electron beam welded Al-alloy 7020. J Mater Sci 42: 7154–7161
8. Cam G, Ventzke V, Dos Santos JF, Kocak M, Jennequin G, Gonthier-Maurin P (1999) Characterisation of electron beam welded aluminium alloys. Sci Technol Weld Join 4:317–323
9. Pakdil M, Çam G, Koçak M, Erim S (2011) Microstructural and mechanical characterization of laser beam welded AA6056 Al-alloy. Mater Sci Eng A 528(24):7350–7356
10. Çam G, Ventzke V, dos Santos JF, Koçak M, Jennequin G, Gonthier-Maurin P, Penasa M, Rivezla C (2000) Characterization of laser and electron beam welded Al-alloys. Prakt Metallogr 37(2): 59–89
11. Çam G, Mıstıkoğlu S (2014) Recent developments in friction stir welding of Al-alloys. J Mater Eng Perform (JMEPEG) 23(6):1936–1953
12. Çam G (2011) Friction stir welded structural materials: beyond Al-alloys. Int Mater Rev 56(1):1–48
13. Ipekoglu G, Kiral BG, Erim S, Cam G (2012) Investigation of the effect of temper condition on the friction stir weldability of AA7075 Al- alloy plates. Mater Tehnol 46:627–632
14. İpekoğlu G, Erim S, Çam G (2014) Effects of temper condition and post weld heat treatment on the microstructure and mechanical properties of friction stir butt welded AA7075 Al-alloy plates. Int J Adv Manuf Technol 70(1):201–213
15. İpekoğlu G, Çam G (2014) Effects of initial temper condition and postweld heat treatment on the properties of dissimilar friction-stir-welded joints between AA7075 and AA6061 aluminum alloys. Metall Mater Trans A 45A(7):3074–3087
16. Szymanski Robert T (2011) Friction stir welding of dissimilar metals, US Patent 20110214799
17. Bozkurt Y, Salman S, Çam G (2013) The effect of welding parameters on lap-shear tensile properties of dissimilar friction stir spot welded AA5754-H22/2024-T3 JOINTS. Sci Technol Weld Join 18(4):337–345
18. Dunkerton SB (1982) Report 201/1982. TWI, Abington Hall, Cambridge
19. Dunkerton SB (1983) Report 229/1982. TWI, Abington Hall, Cambridge
20. Hartwig H, Kouptsidis JS (1977) Proc. 7th Int. Vacuum cong. and 3rd conf. on solid surfaces. Vienna, Osterreichshe Sutdeingesellschaft fur Atomenergie. pp. 259–262
21. Sassani F, Neelam JR (1988) Weld J 66(11):264–270
22. Grong O (1994) Metallurgical modelling of welding. The Institute of Materials, London
23. Grong O (1997) Metallurgical modelling of welding, 2nd edn. Maney, London
24. Wang KK (1975) Friction welding. Welding Research Bulletin, New York, p 204
25. Mumin S (2004) Simulation of friction welding using a developed computer program. J Mater Process Technol 153–154:1011–1018. doi:10.1016/j.jmatprotec.2004.04.287
26. Subhash Chander G, Madhusudhan Reddy G, Tagore GRN (2013) Influence of process parameters on impact toughness and hardness of dissimilar AISI 4140 and AISI 304 continuous drive friction welds. Int J Adv Manuf Technol 64(9–12):1445–1457
27. Anderson (1988) Inspection of metals: destructive testing. ASM international, USA
28. Akbarimousavi SAA, Goharikia M (2011) Investigation on the mechanical properties and microstructure of dissimilar cp-titanium and AISI 316L austenitic stainless steel continuous friction welds. Mater Des 32:3066–3075